

Cheminformatics-Driven Discovery of Selective, Nanomolar Inhibitors for Staphylococcal Pyruvate Kinase

Peter Axerio-Cilies,^{†,‡} Raymond H See,^{†,⊥} Roya Zoraghi,[†] Liam Worrall,^{||} Tian Lian,[†] Nikolay Stoykov,[§] Jihong Jiang,[†] Sukhbir Kaur,[†] Linda Jackson,[†] Huansheng Gong,[†] Rick Swayze,[†] Emily Amandoron,[†] Nag S. Kumar,[▽] Anne Moreau,[▽] Michael Hsing,^{†,‡} Natalie C. Strynadka,^{||} William R. McMaster,^{†,⊥} B. Brett Finlay,^{||,#,¶} Leonard J Foster,^{§,||} Robert N. Young,[▽] Neil E. Reiner,^{+,†,#,*} and Artem Cherkasov^{+,†,‡,*}

[†]Division of Infectious Diseases, Department of Medicine, [§]Centre for High-Throughput Biology, ^{||}Department of Biochemistry and Molecular Biology, [#]Department of Microbiology and Immunology, and [¶]Michael Smith Laboratories, University of British Columbia, Vancouver, BC, Canada

[‡]Vancouver Prostate Centre, Vancouver, BC, Canada

[⊥]University of British Columbia Centre for Disease Control, Vancouver, BC, Canada

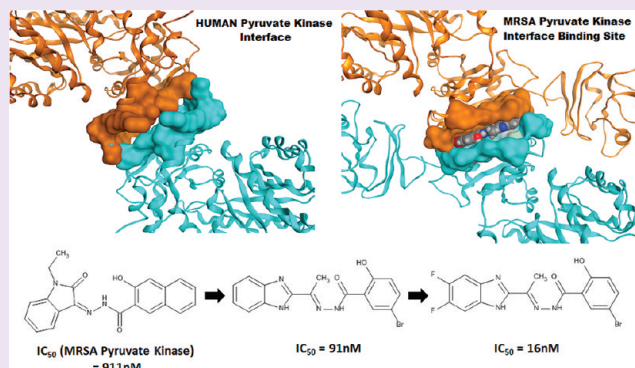
[▽]Department of Chemistry, Simon Fraser University, Burnaby, BC, Canada

Supporting Information

ABSTRACT: We have recently mapped the protein interaction network of methicillin-resistant *Staphylococcus aureus* (MRSA), which revealed its scale-free organization with characteristic presence of highly connected hub proteins that are critical for bacterial survival. Here we report the discovery of inhibitors that are highly potent against one such hub target, staphylococcal pyruvate kinase (PK). Importantly, the developed compounds demonstrate complete selectivity for the bacterial enzyme compared to all human orthologues.

The lead 91nM inhibitor IS-130 has been identified through ligand-based cheminformatic exploration of a chemical space around micromolar hits initially generated by experimental screening. The following crystallographic study resulted in identification of a tetrameric MRSA PK structure where IS-130 is bound to the interface between the protein's subunits. This newly described binding pocket is not present in otherwise highly similar human orthologues and can be effectively utilized for selective inhibition of bacterial PK. The following synthetic modifications of IS-130, guided by structure-based molecular modeling, resulted in the development of MRSA PK inhibitors with much improved antimicrobial properties.

Considering a notable lack of recent reports on novel antibacterial targets and cognate antibacterial compounds, this study provides a valuable perspective on the development of a new generation of antimicrobials. Equally noteworthy, the results of the current work highlight the importance of rigorous cheminformatics-based exploration of the results of high-throughput experiments.



INTRODUCTION

The vast majority of antibiotics currently in use act on bacteria-specific targets to avoid essential housekeeping proteins that have homologues in humans. Such specificity reduces the potential for toxicity but severely limits the available targets for drug design and may also be a contributing factor to ever growing antibiotic resistance among human pathogens.

In response to antibiotic pressure, bacteria have developed numerous resistance mechanisms,¹ rapidly diminishing the effectiveness of conventional antimicrobials. One major example of this is methicillin-resistant *Staphylococcus aureus* (MRSA)² among many others.³ Indeed, MRSA infections now

represent a majority of hospital-acquired infections, which are beginning to penetrate into the community at a large scale and result in an annual death toll in the United States that exceeds that of AIDs.⁴ Thus, new approaches are needed to confront the challenges of rapidly emerging antibiotic resistance and to merge a pipeline of novel, highly effective antimicrobials.

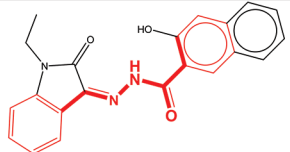
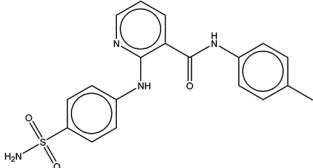
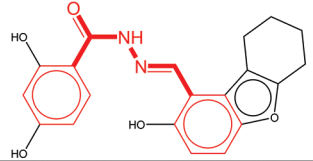
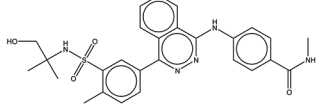
Recent progress in high-throughput technologies has enabled the detection of protein–protein interactions on a proteome-wide

Received: September 9, 2011

Accepted: November 8, 2011

Published: November 8, 2011

Table 1. Four Most Potent MRSA PK Inhibitors Identified by High-Throughput Screening

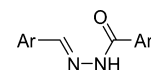
ID	Structure	IC ₅₀ MRSA PK, μM	MIC MRSA μM	I	II	III	IV	V
IS-63		0.911	>500	83.9	15	1.3	13.5	22.2
IS-168				79.5	17.6	12.6	30.6	24.7
IS-53				77.8	39.3	57.5	78.1	87.8
IS-165				54.6	25.8	8.3	15.3	9.4

that have been selected from the ZINC database¹² to justify “drug-like”, “antibiotic-like”, and “bacterial-metabolite-like” criteria,¹³ we have conducted their experimental evaluation for inhibitory activity against the MRSA PK. After eliminating active compounds that demonstrate general aggregating behavior, four individual chemicals have been characterized as potential MRSA PK binders exhibiting a significant effect ($\geq 50\%$ inhibition at $10 \mu\text{M}$) on MRSA PK enzymatic activity (Table 1). Subsequently, these compounds were screened against human PK isoforms (M1, M2, R, and L) in a search for molecules that selectively interact with the bacterial PK. Table 1 provides a selected subset of the most active compounds (the entire list of tested compounds *via* high-throughput screening (HTS) can be found as Supplementary Table S1). This resulted in the characterization of an acyl hydrazone-based compound IS-63 as the most potent and selective MRSA PK inhibitor (with more than 45-fold selectivity over the human PKs). Three other hit compounds, IS-53, IS-165, and IS-168 (Table 1), demonstrated less tolerable levels of activity against human PK isoforms (see Supplementary Table S2 for screening details).

The consecutive titration of the inhibitory effect of IS-63 on the MRSA PK (Figure 2) established the corresponding IC₅₀ value as $\sim 0.911 \mu\text{M}$ (Table 1). However, in a cell-based assay IS-63 demonstrated less than 10% inhibition of growth of intact *S. aureus* cultures when administered at $100 \mu\text{M}$. (Figure 2). We hypothesized that the lack of *in vivo* activity of IS-63 against *S. aureus* might be due to poor cell penetration and decided to identify chemically similar substances that may exhibit better MIC properties, while maintaining high *in vitro* inhibition and selectivity.

Similarity Search for Analogues of IS-63. When analyzing hit compounds we have noted that two out of four

identified active chemicals (compounds IS-63 and IS-53) contain a common structural motif:



Thus, we have used this structural query to search through the updated ZINC-8.0 database.¹² In the following step, the identified chemicals, possessing the desired substructure, have been compared to IS-63 using molecular Fingerprint-based similarity to ensure their overall structural resemblance. The selected ZINC compounds that justified 0.60 or 60% Tanimoto similarity criteria to IS-63 (Supplementary Table S1) have further been tested for *in vitro* inhibitory activity against the MRSA PK.

Out of 56 tested ZINC chemicals (Supplementary Table S3) containing the common substructure and justifying $>60\%$ similarity to IS-63 criteria, seven demonstrated $>50\%$ inhibition of MRSA PK at $10 \mu\text{M}$ concentration. The corresponding substances are collected into Table 2 along with their inhibition characteristics for the MRSA and human PK isoforms. The common structural motif present in the compounds' 2D structures is highlighted in red.

Notably, one analogue of the initial IS-63 hit, compound IS-130, demonstrated complete inhibition of the MRSA PK at $10 \mu\text{M}$ and, when titrated, yielded an IC₅₀ value of $0.09 \mu\text{M}$ (compared to $0.9 \mu\text{M}$ for the parental substance IS-63) while maintaining complete selectivity for the bacterial PK (Figure 2). This represented a significant improvement in the desired biological activity; moreover, as also shown in Figure 2, IS-130 exhibited no growth-inhibition effects on human HeLa cells when tested at up to $500 \mu\text{M}$ concentration.

These findings demonstrate that compound IS-130, identified merely on the basis of chemical similarity to IS-63, possesses significantly improved selectivity and 10-fold improved activity toward the target compared to the parental hit. However, its inhibitory effect on the growth of the MRSA

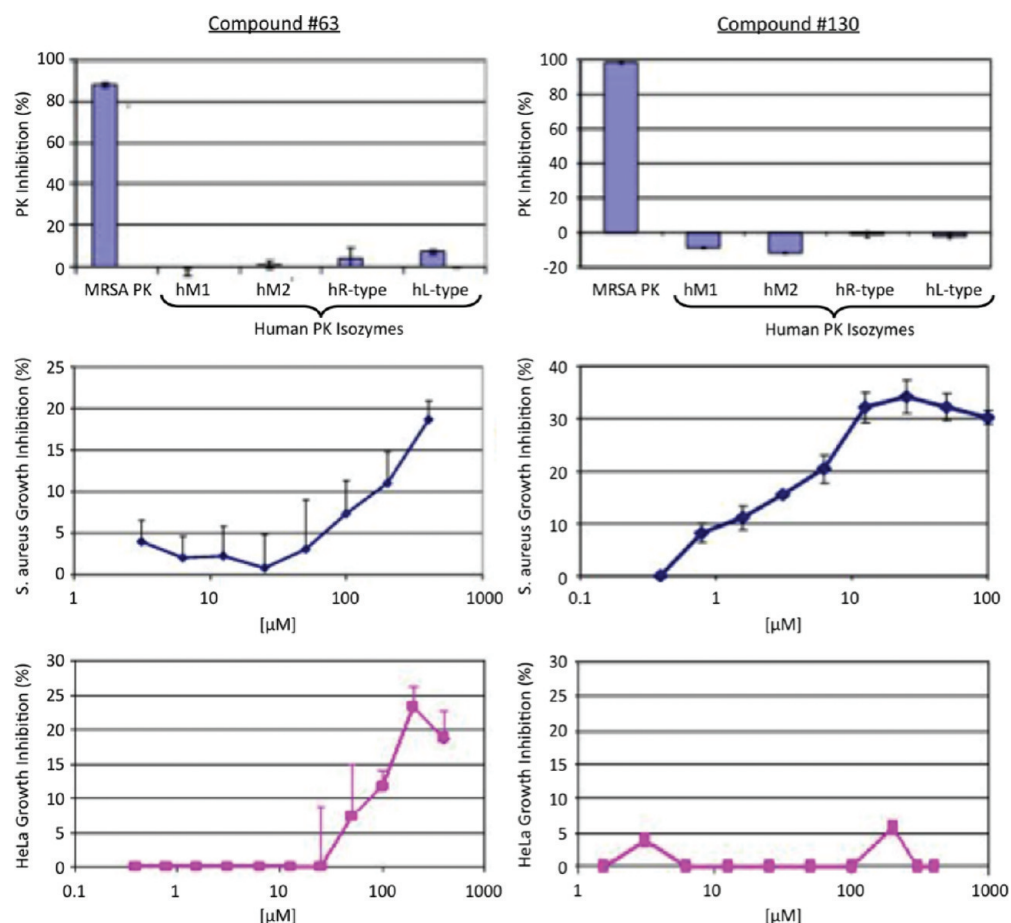


Figure 2. Effect of compounds IS-63 and IS-130 on MRSA252 PK. (Top panel) Inhibition of enzymatic activity of the MRSA and human PK isoforms by compounds IS-63 and IS-130 when administered at 10 μM . (Middle panel) Concentration-dependent effect of compounds IS-63 and IS-130 compounds on *S. aureus* culture growth. (Bottom panel) Toxicity effect of compounds IS-63 and IS-130 on human HeLa cells.

cell culture was still poor (MIC >500 μM). That could be attributed to the lack of stability of IS-130 over a 24 h period and/or low bacterial cell penetration. The relative polarity and basicity of the benzimidazole moiety in IS-130 could also contribute to the low cell permeability.

Co-crystallization of MRSA PK with IS-130. To verify that the lead compound does interact with the MRSA PK directly, we resolved the crystal structure of the protein complexed with the IS-130 molecule (deposited to the Protein Data Bank with PDB ID 3T0T) (Figure 3, Supplementary Table S4 for crystallographic data). The determined structure revealed that the inhibitor binds to a previously uncharacterized protein pocket located at an interface between two PK subunits (Figure 4a). When the experimentally resolved structures of the MRSA and human PKs were superimposed, we were able to identify 10 amino acids in each subunit of the enzyme (highlighted as Thr348, Thr353, Ser354, Ala358, Ile361, Ser362, His365, Thr366, Asn369, and Leu370 in Figure 4a) that contribute to the formation of the actual binding pocket. In the bacterial protein this site is accessible for small molecules, but in the human version it is blocked by five amino acid residues: Glu418-B, Arg399-A,B and Arg400-A,B (Figure 4a). This obstruction in the human PK protein coupled with the overall low sequence conservation in the interface region explains differentiated binding of small molecules (Figure 4b and Supplementary Figure S1). Considering that previous studies had indicated that conformational changes in intrasubunit

interfaces of PK can disrupt its enzymatic activity,¹⁴ we could hypothesize that the identified MRSA PK binding site represents a valid target.

Another very important observation resulting from the resolution of the structure of the MRSA PK/IS-130 complex is that merely ligand-based screening allowed discovery of the highly promising hit IS-130 that could not be otherwise identified by structure-based *in silico* methods, such as docking. The main reason for that is the fact that the structural pocket located between the subunits of PK has never been described or characterized as a potentially suitable site for small molecule binding. This example highlights the importance of cheminformatics-based exploration of chemical space around initial experimental hits, *i.e.*, identification of structurally or topologically similar compounds that may also possess the desired (and even superior) activity.

The experimentally identified orientation of IS-130 inside the MRSA PK is shown in Figure 4c along with the corresponding hydrogen bonding patterns occurring within the interface-binding cavity. This demonstrates that the identified 91nM inhibitor is anchored by 4 main hydrogen bonds; the 2D schematic (Figure 4c) illustrates that the sp^2 hybridized nitrogen of the hydrozone moiety, the sp^3 hybridized nitrogen from the indole moiety, and the linker carbonyl functional group all interact with the Ser362-A residue. This carbonyl group was also seen to be engaged with Ser362-B, which is located just adjacent to Ser362-A (A and B notations

Table 2. MRSA PK Inhibitors Identified through Structural Similarity to IS-63^a

ID	Structure	IC ₅₀ MRSA PK, μM	MIC MRSA μM	I	II	III	IV	V	Tanimoto to IS-63
IS-130		0.091	>500	98.5	-8.7	-11.9	-1.2	-2.1	0.63
IS-176				78.8	10.9	10.2	7.3	-4.7	0.72
IS-134				78.3	22.8	26.7	15.7	20.8	0.76
IS-193				71.1	-1.7	2.2	9.8	0.9	0.60
IS-173				66.4	13.0	11.8	7.1	-1.0	0.76
IS-152				60.6	3.6	25.3	5.6	12.3	0.64
IS-136				50.0	10.4	10.2	0.4	0.8	0.70

^aPercent inhibition of (I) MRSA PK, 10 μM ; (II) human PK M1 isoform, 10 μM ; (III) human PK M2 isoform, 10 μM ; (IV) human PK R-type isoform, 10 μM ; (V) human PK L-type isoform, 10 μM .

correspond to different MRSA PK subunits). These serine residues are of particular interest as they are not conserved in human PK and thus are likely to further influence the selectivity of the compound for bacterial PK (Figure 4b and Supplementary Figure S1). In addition, the hydroxyl group of IS-130 appeared to hydrogen bond with His365-B, which is also a residue unique to the bacterial protein (Figure 4b and Supplementary Figure S1). Figure 4c also shows that strong hydrophobic interactions were observed between *p*-bromine and Ile361-B, Ala358-B, and Leu370-A residues (while among these only Leu370-A was noted to be unique to bacterial PK).

Taken together, these findings show that the selectivity of the lead compound for bacterial PK can be attributed to poorly conserved interface residues, which in the case of MRSA PK interacted directly with the ligand. We anticipated that further exploitation of these distinctive regions of the interface can reinforce selectivity of drug candidates toward the bacterial target.

Optimization of IS-130 Lead Compound. In order to improve the MIC characteristics of the lead compound IS-130, we have investigated possible structure–activity relationships for its derivatives. To ensure that the binding modes of the derivatives are consistent with IS-130, we have also conducted molecular docking of the corresponding substances to the site (Supporting Information). In particular, using the resolved crystal structure of IS-130 bound to the interface pocket of MRSA PK, we have explored several structural alterations to the parental substance summarized in Table 3.

Thus, utilizing electronic homology, we have replaced one indole sp^2 hybridized nitrogen in IS-130 to sp^2 carbon to reduce the basicity of compounds and to facilitate their cell penetration. The resulting chemicals NSK-466, AM-160, AM-213, AM-168, NSK-477, AM-165, NSK-577, and NSK-515 are listed in Table 3 along with their measured abilities to inhibit the MRSA PK enzymatic activity and *S. aureus* cell culture growth. As the listed IC₅₀ values indicate, the replacement of an imidazole feature in IS-130 with an indole fragment resulted in

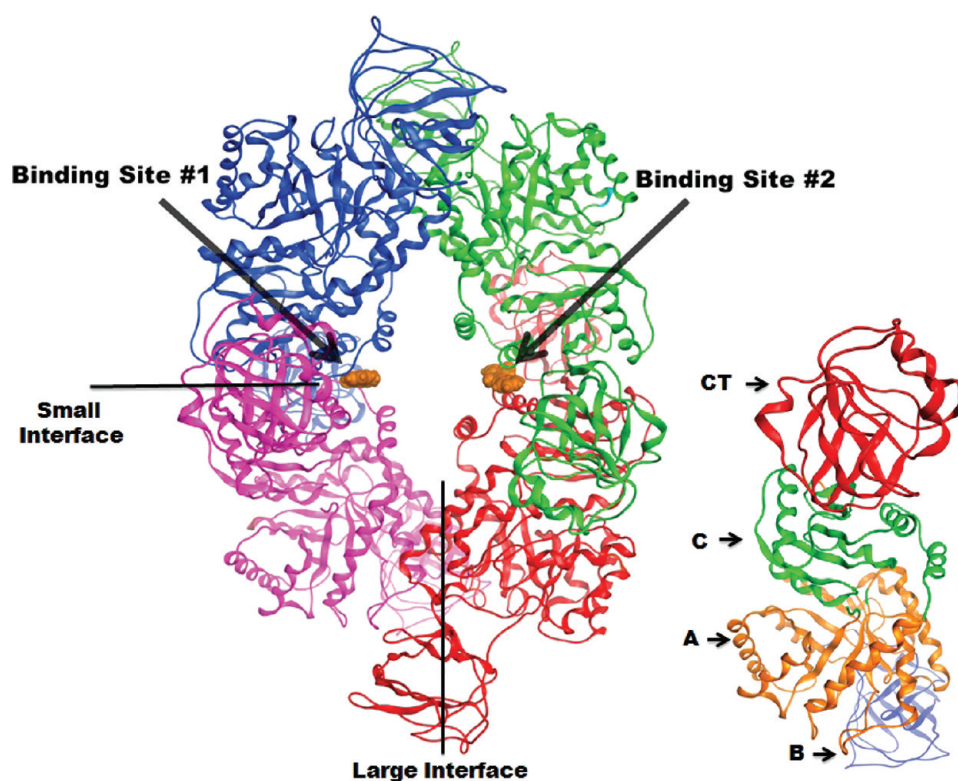


Figure 3. Crystal structure of MRSA252 pyruvate kinase. (Left) Resolved structure of MRSA252 pyruvate kinase tetramer showing the domain boundaries and tetramer architecture. Each monomer has been colored to facilitate the identification of the small interface (arrows). The two binding sites are located at the small interface that sits in between two α helices formed by two PK monomers. (Right) The domains of MRSA pyruvate kinase: A-domain (A), B-domain (B), C-domain (C), and C-terminal (CT).

generally decreased IC_{50} values that perhaps could be attributed to increased hydrophobic interactions with Ile371 side-chain of one of the PK subunits.

We also carried out some limited exploration of a role of halogen substitutions at the R2 and R1 positions of the indole moiety. The resolved X-ray structure of the IS-130 complex revealed that the conformational space between position R1 and R2 and the protein is fairly tight, showing only ~ 4 Å distance between them. Although this area is somewhat restricted, the accommodation of small halogen atoms such as fluorine can be beneficial. As shown in Table 3, the presence of fluorine in R2 may account for the improved IC_{50} of 16 nM for AM-213. The introduction of bulkier chlorine substituents in R1 position seemed to further improve overall target binding of the compounds likely caused by increased van der Waals interactions with Ile361, Leu370, and Ala358 residues (Supplementary Figures S2 and S3). Interestingly, the fact that the substitution of a common methyl group in the R3 position with a larger hydrophobic ethyl moiety (AM-168) (Supplementary Figure S3) led to a notable improvement in MIC could be attributed to overall increase of ligand hydrophobicity and strengthened van der Waals interaction of R3 with His365 residues from both PK subunits. Similarly, introduction of a methyl groups to R4 position in compounds NSK-477, AM-165, NSK-577, and NSK-515 resulted in much improved cell growth inhibition, which highlights the importance of maintaining higher hydrophobicity of the studied compounds. It was also noted that there were three unique hydrogen bonding patterns observed among the synthetic derivatives (Supplementary Figure S3). More specifically, the indole nitrogen, sp^2 nitrogen, carbonyl, and the hydroxyl group

all play an important role in the protein–ligand interactions. These interactions are mediated on the basis of whether the indole nitrogen is methylated or whether a bulkier group is attached to the sp^2 carbon such in the case of AM-168 (Supplementary Figure S3).

As data in Table 3 indicate, the derivative NSK-515 demonstrated the most balanced inhibition of MRSA PK enzymatic activity and *S. aureus* culture among the studied compounds, with the corresponding IC_{50} and MIC values being 0.18 and 3.1 μM , respectively. Importantly, this lead candidate (as well as other chemicals from Table 3) also demonstrated >100-fold selectivity toward staphylococcal enzyme, compared to its close human orthologues.

Taken together, the findings of the initial SAR exploration of synthetic derivatives of lead compound IS-130 demonstrate that its discrete structural modifications were able to enhance potency against the MRSA PK. Ongoing work is aimed at gaining better insight into the SAR of the developed MRSA PK inhibitors and, in particular, at optimizing properties in terms of inhibition of bacterial growth.

Mode of Action of IS-130. The MRSA pyruvate kinase protein functions as a homotetramer where each subunit consists of an A-domain, B-domain, C-domain, and an extra C-terminal region (CT) (Figure 3). The tetramerization of the protein is facilitated by the interactions between the A- and C-domains, whereby the adjacent C-domains form the C–C small interface (Figure 3).¹⁴ The established crystal structure of the MRSA PK complexed with a compound IS-130 reveals its direct binding to the C-domain interface (Figure 3). Recently, Morgan *et al.* outlined the allosteric mechanism of regulation of pyruvate kinase (PK) from *Leishmania mexicana*.¹⁵ It has been

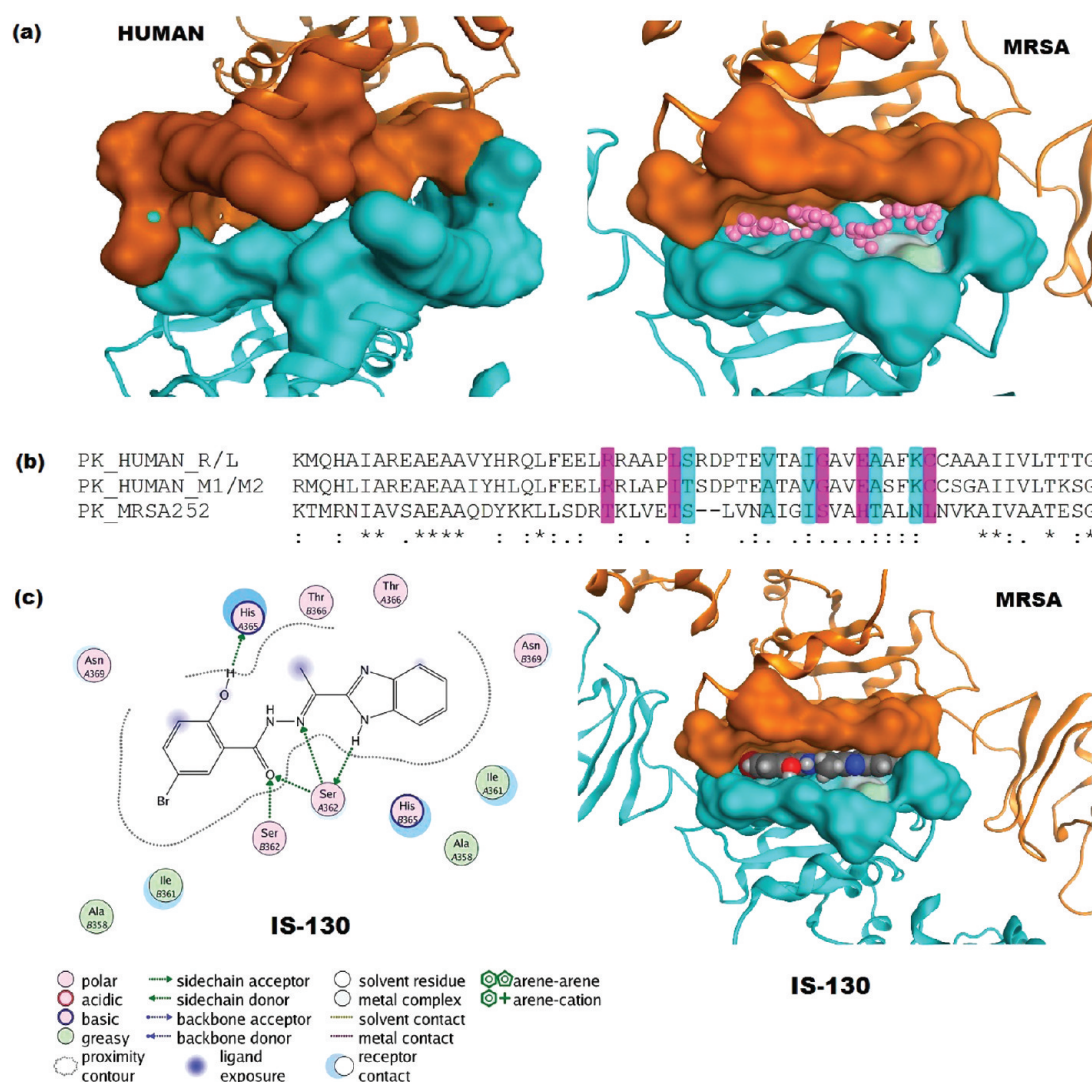


Figure 4. Differential region between MRSA252 PK and human PK. (a) Structures of the interface-binding site for MRSA and human PK. Pink spheres show the interface cavity in MRSA and human. The MRSA PK model shows an accessible binding pocket located at the interface of two PK monomers (right). In contrast, the pocket in human PK is partially obstructed by five amino acid residues (Glu418-B, Arg399-A,B, and Arg400-A,B (left)). (b) Sequence alignment showing the C-domains of MRSA252 PK and human isoforms. Highlighted residues are denoted to be the interface region for pyruvate kinase (PK) from *Staphylococcus aureus* and the two isozymes R/L and M1/M2 from *Homo sapiens*. The poorly conserved residues between MRSA and human PKs are highlighted purple. The full sequence alignment of both the human isozymes and MRSA252 are shown in Supporting Information. Sequences were aligned by using ClustalW2 software.²⁵ (c) Binding mode of compounds IS-130 at the interface binding site. A two-dimensional map of the binding interactions between IS-130 and the interface site based on its co-crystallization with MRSA PK. Green arrows depict hydrogen-accepting interactions between IS-130 and MRSA PK residues from the interface (left). Binding orientation of IS-130 within the interface-binding pocket is based on the protein–ligand crystal structure (right).

Table 3. PK Inhibitory Activity and Antimicrobial Activity of Selected Synthesised Derivatives of Compound IS-130

derivatives	IC ₅₀ (μM)	MIC (μM)	R1	R2	R3	R4
NSK-466	0.084	>500	H	H	CH ₃	H
AM-160	0.045	>500	F	H	CH ₃	H
AM-213	0.016	>200	F	F	CH ₃	H
AM-168	0.114	25	H	H	C ₂ H ₅	H
NSK-477	0.381	12	H	H	CH ₃	CH ₃
AM-165	0.165	6.2	F	H	CH ₃	CH ₃
NSK-577	0.228	3.1	Cl	H	CH ₃	CH ₃
NSK-515	0.185	3.1	Br	H	CH ₃	CH ₃

demonstrated that transition between active and inactive forms of the PK is facilitated by symmetrical rocking motion of A- and C-core domains in the PK subunits.¹⁵ The functional tetramer is formed when four pairs of salt bridges are formed across C–C small interfaces whereby A- and C-domain cores become locked in a rigid configuration corresponding to an active form of the enzyme.¹⁵ Thus, it is feasible to speculate that compound IS-130 can interfere with the formation of these crucial salt bridges and prevent the formation of an active configuration of the enzyme.

CONCLUSION

To summarize the findings of the current study, it is possible to stipulate that essential bacterial hub proteins such as pyruvate kinase represent attractive drug targets for developing small-molecule antimicrobials. Furthermore, the synergy between high-throughput screening techniques and methods of cheminformatics allows the discovery of highly promising drug candidates that are possibly capable of addressing the growing problem of drug resistance among bacterial pathogens.

METHODS

ZINC Chemical Database Preparation. Approximately 200 commercially available structures from the ZINC-8.0 virtual screening library¹² were downloaded in SD format and imported into MOE (Molecular Operating Environment, Version 2009.10) database environment.¹⁶ The structures were “washed” by removing all inorganic components and by adjusting ionization states to pH = 7.0 condition. Furthermore, the database entries were energy-minimized using the MMFF94x force field.¹⁷

Similarity Search. The 2D similarity score for the lead compounds were calculated by means of a Tanimoto coefficient and using MACCS fingerprints^{18,19} as implemented by MOE. These fingerprints contain 166 bits indicating the presence of specified structural fragments in the molecular graph representation. The similarity search was conducted against the ZINC library.¹²

A Tanimoto similarity measure, T_c , was calculated for each ligand based on the formula

$$T_c(A, B) = \frac{N_{AB}}{N_A + N_B - N_{AB}}$$

where N_{AB} is the number of bits that are set on in both fingerprints, and N_A and N_B refer to the number of bits that are set on in A and B, respectively. Identical fingerprints have a T_c value of 1, whereas nonoverlapping fingerprints are given a T_c value of 0.²⁰ A cutoff value of $T_c = 0.60$ (60% similarity level) was imposed.

The substructure search was carried out using custom SVL scripts for the MOE.¹⁶

PK Enzymatic Assays and Cell-Based Screens. Each compound that justified the described cheminformatics criteria was purchased and tested in a PK enzyme colorimetric assay. Expression and purification of recombinant histidine-tagged MRSA and human PK isoforms (M1, M2, R, and L) were performed as previously described.²¹ Human M2 PK isoform was cloned using the primers hM2F 5'-GATCATATGATGTCGAAGCCCCATAGTGAAGCC-3' and hM2R 5'-GTTCTCGAGTCACGGCACAGGAACAACACGCATG-3'. The resulting PCR fragments for each construct were cloned into the *NdeI* and *XhoI* unique sites of the bacterial expression vector pET-28a (+) (*Novagen*). This step resulted in the plasmid pET-28M2, which generated N-terminal His-tagged recombinant human M2 PK. The sequence and the correct reading frame of all constructs were verified by sequencing. PK enzymatic activity was measured using a continuous colorimetric assay coupled to lactate dehydrogenase as previously described.²¹ PK activity proportional

to the rate of change at 340 nm was expressed as specific activity ($\mu\text{mol}/\text{min}/\text{mg}$), which is defined as the amount of PK that catalyzes the formation of 1 μmol of either product per minute. Inhibitors were dissolved in DMSO with the final concentration of the solvent never exceeding 1% of the assay volume. IC_{50} values were calculated by curve fitting on a four-parameter dose–response model with variable slope using Graphpad Prism 5.0 (GraphPad Software Inc., La Jolla, CA). In all studies, less than 10% of total PEP was exhausted during the reaction. Reactions were performed at 30 °C for 5 min. All values determined represent three measurements, each in triplicate unless mentioned otherwise. Any compounds showing 50% or more inhibition of the MRSA PK activity in the primary screen were then screened against 4 human isozymes (M1, M2, L, and R) in the secondary assay.²²

All inhibitors initially considered as potent and selective were then tested for inhibition of *S. aureus* growth using a 24-h MIC (minimum inhibitory concentration) assay. Finally, human HeLa cells were used to evaluate whether PK inhibitory compounds were cytotoxic by using CellTiter 96 AQueous One Solution Cell Proliferation kit (Promega). Those compounds that showed potency in enzymatic and cell-based assays were rescreened by an *in silico* similarity search method to find analogues that exhibit a higher potency and improvement in *S. aureus* cell penetration and growth inhibition. Structures and measured biological activity of all initially tested compounds and ^1H NMR spectra of IS-63 and IS-130 compounds are shown in Supplemental Figures S4 and S5.

Molecular Docking. Molecular docking experiments were carried out to ensure that the binding poses for the IS-130 analogues were consistent in the interface binding site and to propose possible structural modifications that can be done to optimize IS-130 lead structure. The detailed protocol is described in Supporting Information.

Syntheses of IS-130 Analogues. Syntheses of the hydrazides NSK-466, AM-160, AM-168, AM-213, NSK-515, NSK-577, and AM-165 are described in detail in Supporting Information.

NMR Experiments. ^1H and ^{13}C NMR spectra were recorded with either Bruker Avance II 600 MHz, Bruker Avance III 500 MHz, or Bruker Avance III 400 MHz instruments. Processing of the spectra was performed with MestRec software. The high-resolution mass spectra were recorded in positive ion mode with an ESI ion source on an Agilent Time-of-Flight LC/MS mass spectrometer.

Analytical thin-layer chromatography (TLC) was performed on aluminum plates precoated with silica gel 60F-254 as the absorbent. The developed plates were air-dried, exposed to UV light and/or dipped in KMnO_4 solution and heated. Column chromatography was performed with silica gel 60 (230–400 mesh). Purity checks for all final compounds were completed by analytical reverse-phase HPLC utilizing a Dikma Technologies Inspire C18 Inspire C18 5 μm , 4.6 mm i.d. (150 mm \times 4.6 mm) using an Agilent Technologies 1100 Series with an Agilent VWD (MeOH/ H_2O -0.1% TFA, 80–95% for 5 min, followed by isocratic elution at 95% for another 3 min, 1.5 mL/min, 254 nm detection for 10 min).

Crystallization and Refinement. *S. aureus* PK was purified and crystallized as previously described.²² For co-crystallization experiments, 50 mM IS-130 in 100% DMSO was diluted 100 \times in protein solution, centrifuged, and set up. Data were collected at station 08ID-1 of the Canadian Light Source (Saskatoon, Canada) at a wavelength of 0.91839 Å and temperature of 100 K. Data processing and refinement were carried out as previously described.²² See Supplementary Table S4 for data processing and refinement statistics. Model validation was carried out with MolProbity²³ with 92.1% of residues in the favored region of the Ramachandran map and 1.5% outliers. Data collection at the Bromine edge allowed calculation of an anomalous difference map and confirmation of the ligand binding position. Structure factors and coordinates have been deposited to the Protein Data Bank with PDB ID 3T0T, and the crystallographic data are shown in Supplementary Table S4.

■ ASSOCIATED CONTENT

■ Supporting Information

Structures and measured biological activity of all initially tested compounds; H^1 NMR spectra of IS-63 and IS-130 compounds; crystallographic data of MRSA252 pyruvate kinase co-crystallized with IS-130; biological screening details; sequence alignment between human isoforms and bacterial MRSA252 pyruvate kinase; synthesis of IS-130 derivatives and details of their interactions within the binding site. This material is available free of charge *via* the Internet at <http://pubs.acs.org>.

Accession Codes

Protein Data Bank ID 3T0T.

■ AUTHOR INFORMATION

Corresponding Author

*E-mail: archerkasov@prostatecentre.com.

Author Contributions

[†]These authors contributed equally to this work.

■ ACKNOWLEDGMENTS

This work was supported by funding from Genome Canada and Genome British Columbia, Vancouver General Hospital & University of British Columbia Hospital Foundation, and SARS Accelerated Vaccine Initiative through the PRoteomics for Emerging PATHogen REsponse (PREPARE) Project. Computer equipment in PREPARE Project's Computational Genomics research were also supported by in-kind contribution from IBM Healthcare and Life Sciences. N.S.K., A.M., and R.N.Y. acknowledge support from the Natural Sciences and Engineering Research Council of Canada and Simon Fraser University. We would like to thank L. Cantley and M. Vander Heiden from Department of Systems Biology, Harvard Medical School for providing us with M1, R, and L human PK constructs in pET-28-a(+) vectors.

■ ABBREVIATIONS

MRSA: methicillin-resistant *Staphylococcus aureus*; PK: pyruvate kinase; PIN: protein interaction network; MIC: minimal inhibiting concentration; ATP: adenosine triphosphate; ADP: adenosine diphosphate

■ REFERENCES

- (1) Wright, G. D. (2003) Mechanisms of resistance to antibiotics. *Curr. Opin. Chem. Biol.* 7, 563–569.
- (2) Rybak, M. J. (2004) Resistance to antimicrobial agents: and update. *Pharmacotherapy* 24, 203–215.
- (3) Peleg, A. Y., and Hooper, D. C. (2010) CURRENT CONCEPTS Hospital-acquired infections due to Gram-negative bacteria. *New Engl. J. Med.* 362, 1804–1813.
- (4) Cuddy, S. M. (2008) Methicillin-resistant *Staphylococcus aureus*: a new pandemic? Plastic surgical nursing. *Plast. Surg. Nurs.* 28, 168–169.
- (5) Butland, G., Peregrin-Alvarez, J. M., Li, J., Yang, W. H., Yang, X. C., Canadian, V., Starostine, A., Richards, D., Beattie, B., Krogan, N., Davey, M., Parkinson, J., Greenblatt, J., and Emili, A. (2005) Interaction network containing conserved and essential protein complexes in *Escherichia coli*. *Nature* 433, 531–537.
- (6) Gavin, A. C., Aloy, P., Grandi, P., Krause, R., Boesche, M., Marzioch, M., Rau, C., Jensen, L. J., Bastuck, S., Dumpelfeld, B., Edlmann, A., Heurtier, M. A., Hoffman, V., Hoefert, C., Klien, K., Hudak, M., Michon, A. M., Schelder, M., Schirle, M., Remor, M., Rudi, T., Hooper, S., Bauer, A., Bouwmeester, T., Casari, G., Drewes, G., Neubauer, G., Rick, J. M., Kuster, B., Bork, P., Russell, R. B., and Superti-Furga, G. (2006) Proteome survey reveals modularity of the yeast cell machinery. *Nature* 440, 631–636.

- (7) Hermjakob, H., Montecchi-Palazzi, L., Lewington, C., Mudali, S., Kerrien, S., Orchard, S., Vingron, M., Roechert, B., Roepstorff, P., Valencia, A., Margalit, H., Armstrong, J., Bairoch, A., Cesareni, G., Sherman, D., and Apweiler, R. (2004) IntAct: an open source molecular interaction database. *Nucleic Acids Res.* 32, D452–D455.

- (8) Barabasi, A. L., and Oltvai, Z. N. (2004) Network biology: Understanding the cell's functional organization. *Nat. Rev. Genet.* 5, 101–U115.

- (9) Cherkasov, A., Hsing, M., Zoraghi, R., Foster, L. J., See, R. H., Stoynov, N., Jiang, J., Kaur, S., Lian, T., Jackson, L., Gong, H., Swayze, R., Amandoron, E., Hormozdiari, F., Dao, P., Sahinalp, C., Santos-Filho, O., Axerio-Cilies, P., Byler, K., McMaster, W. R., Brunham, R. C., Finlay, B. B., and Reiner, N. E. (2011) Mapping of the protein interaction network in methicillin resistant *Staphylococcus aureus* (MRSA-252) identifies novel high quality drug targets. *J. Prot. Res.* 10, 1139–1150.

- (10) Fraser, H. B., Hirsh, A. E., Steinmetz, L. M., Scharfe, C., and Feldman, M. W. (2002) Evolutionary rate in the protein interaction network. *Science* 296, 750–752.

- (11) Suzuki, K., Ito, S., Shimizu-Ibuka, A., and Sakai, H. (2008) Crystal structure of pyruvate kinase from *Geobacillus stearothermophilus*. *J. Biochem.* 144, 305–312.

- (12) Irwin, J. J., and Shoichet, B. K. (2005) ZINC—a free database of commercially available compounds for virtual screening. *J. Chem. Inf. Model.* 45, 177–182.

- (13) Cherkasov, A. (2006) Can 'Bacterial-Metabolite-Likeness' model improve odds of 'in silico' antibiotic discovery? *J. Chem. Inf. Model.* 46, 1214–1222.

- (14) Tulloch, L. B., Morgan, H. P., Hannaert, V., Michels, P. A. M., Fothergill-Gilmore, L. A., and Walkinshaw, M. D. (2008) Sulphate removal induces a major conformational change in *Leishmania mexicana* pyruvate kinase in the crystalline state. *J. Mol. Biol.* 383, 615–626.

- (15) Morgan, H. P., McNae, I. W., Nowicki, M. W., Hannaert, V., Michels, P. A. M., Fothergill-Gilmore, L. A., and Walkinshaw, M. D. (2010) Allosteric mechanism of pyruvate kinase from *Leishmania mexicana* uses a rock and lock model. *J. Biol. Chem.* 285, 12892–12898.

- (16) Chemical Computing Group, Inc. (2008) *Molecular Operating Environment (MOE) CCG*: Montreal, Quebec, Canada, www.chemcomp.com

- (17) Halgren, T. A. (1995) Merck Molecular Force Field. I-V. *J. Comput. Chem.* 17, 490–641.

- (18) Durant, J. L., Leland, B. A., Henry, D. R., and Nourse, J. G. (2002) Reoptimization of MDL keys for use in drug discovery. *J. Chem. Inf. Comput. Sci.* 42, 1273–1280.

- (19) Sheridan, R. P., Miller, M. D., Underwood, D. J., and Kearsley, S. K. (1996) Chemical similarity using geometric atom pair descriptors. *J. Chem. Inf. Comput. Sci.* 36, 128–136.

- (20) Johnson, M. A., and Maggiora, G. M. (1990) *Concepts and Application of Molecular Similarity*, Wiley, New York.

- (21) Zoraghi, R., See, R. H., Gong, H., Lian, T., Swayze, R., Finlay, B. B., Brunham, R. C., McMaster, W. R., and Reiner, N. E. (2010) Functional analysis, overexpression, and kinetic characterization of pyruvate kinase from methicillin-resistant *Staphylococcus aureus*. *Biochemistry* 49, 7733–7747.

- (22) Zoraghi, R., See, R. H., Axerio-Cilies, P., Kumar, N. S., Gong, H., Moreau, A., Hsing, M., Kaur, S., Swayze, R. D., Worrall, L., Amandoron, E., Lian, T., Jackson, L., Jiang, J., Thorson, L., Labriere, C., Foster, L., Brunham, R. C., McMaster, W. R., Finlay, B. B., Strynadka, N. C., Cherkasov, A., Young, R. N., and Reiner, N. E. (2011) Identification of pyruvate kinase in methicillin-resistant *Staphylococcus aureus* as a novel antimicrobial drug target. *Antimicrob. Agents Chemother.* 55, 2042–2053.

- (23) Chen, V. B., Arendall, W. B. III, Headd, J. J., Keedy, D. A., Immormino, R. M., Kapral, G. J., Murray, L. W., Richardson, J. S., and Richardson, D. C. (2010) MolProbity: all-atom structure validation for macromolecular crystallography. *Acta Crystallogr., Sect. D: Biol. Crystallogr.* 66, 12–21.

(24) Shannon, P., Markiel, A., Ozier, O., Baliga, N. S., Wang, J. T., Ramage, D., Amin, N., Schwikowski, B., and Ideker, T. (2006) Cytoscape: a software environment for integrated models of biomolecular interaction networks. *Genome Res.* 13, 2498–2504.

(25) Altschul, S. F., Gish, W., Miller, W., Myers, E. W., and Lipman, D. J. (1990) Basic local alignment search tool. *J. Mol. Biol.* 215, 403–410.